RSC Advances

PAPER

View Article Online
View Journal | View Issue

Cite this: *RSC Adv.*, 2023, **13**, 11782

Sophorolipid-toluidine blue conjugates for improved antibacterial photodynamic therapy through high accumulation

Xiaoxiao Gu, †[a] Lixian Xu,†[b] Haoyang Yuan,[a] Cailing Li,[a] Juan Zhao,[a] Shuang Li[a] and Dinghua Yu *[a]

Received 12th March 2023
Accepted 10th April 2023

DOI: 10.1039/d3ra01618h

rsc.li/rsc-advances

Anti-bacterial photodynamic therapy is the most promising treatment protocol for bacterial infection, but low accumulation of photosensitizers has seriously hindered their development in clinical application. Here, with inherent outstanding affinity to bacterial cell envelope, sophorolipid produced from *Candida bombicola* has been conjugated to toluidine blue (SL-TB) through amidation reaction. The structure of SL-TB conjugates was identified by ^{1}H-NMR, FT-IR and ESI-HRMS. The interfacial assembly and photophysical properties of SL-TB conjugates have been disclosed through surface tension, micro-polarity, electronic and fluorescence spectra. After light irradiation, the $\log_{10}$ (reduced CFU) of free toluidine blue to *P. aeruginosa* and *S. aureus* were 4.5 and 7.9, respectively. In contrast, SL-TB conjugates showed a higher bactericidal activity, with a reduction of 6.3 and 9.7 $\log_{10}$ units of CFU against *P. aeruginosa* and *S. aureus*, respectively. The fluorescence quantitative results showed that SL-TB could accumulate 2850 nmol/10^{11} cells and 4360 nmol/10^{11} cells by *P. aeruginosa* and *S. aureus*, which was much higher than the accumulation of 462 nmol/10^{11} cells and 827 nmol/10^{11} cells of free toluidine blue. Through the cooperation of triple factors, including sophorose affinity to bacterial cells, hydrophobic association with plasma membrane, and electrostatic attraction, higher SL-TB accumulation was acquired, which has enhanced antibacterial photodynamic efficiencies.

1. Introduction

As demonstrated by the COVID-19 epidemic, pathogenic microorganism infection not only affects food safety and human health, but also the field of medicine and national security, causing huge economic burden and social pressure to human society. Thanks to the emergence of antibiotics, human beings defeated microorganisms in the struggle between human beings and microorganisms.[1,2] However, due to the overuse and misuse of antibiotics, the prevalence of multi-resistant bacteria continues to pose a serious situation in the global healthcare landscape. Especially, the most multi-resistant bacteria associated with severe hospital-acquired infections (HAI) include *Enterococcus faecalis*, *Staphylococcus aureus*, *Klebsiella pneumoniae*, *Acinetobacter baumanii*, *Pseudomonas aeruginosa* and *Enterobacter* sp., which could often result in fatal outcomes.[3] In a recent report from the World Health Organization, multi-resistant bacteria infections would lead to 700 000 deaths annually and the number will be projected to reach 10 million by 2050 due to the absence of efficient treatment protocol for pathogens.[4,5] Therefore, people have been looking for safer and more efficient treatment protocols of bacterial infection without multi-drug resistance development risk.

Among these innovative antibacterial protocols, antibacterial photodynamic therapies (APDT) could be the most promising and characteristic treatment protocols. Due to the multiple action targets to bacterial cells of highly cytotoxic singlet oxygen produced from photodynamic process, antibacterial photodynamic therapy could inactivate a wide range of bacteria with few possibilities to develop drug resistance. However, the photosensitizers couldn't produce efficient antibacterial photodynamic therapy due to inadequate photosensitizers bioaccumulation. The low photosensitizers accumulation and inappropriate distribution could originate from the complex microbial cells structure and biochemical composition, such as proteins, chitin, lipopolysaccharides, and peptidoglycan.[6] This complexity could resist photosensitizers diffusion and accumulation, which has weakened antibacterial photodynamic efficiency. In order to improve photosensitizers accumulation and distribution, it is necessary to select suitable delivery systems that have high affinity to microbial cells surface, such as lipids, proteins, extracellular polysaccharides,

[a]*College of Biotechnology and Pharmaceutical Engineering, Nanjing Tech University, Nanjing 211816, PR China. E-mail: yudh@njtech.edu.cn; Tel: +86-25-58139386*
[b]*Department of Dermatology, The Second Affiliated Hospital of Nanjing Medical University, No.121 Jiangjiayuan Road, Nanjing 210000, P. R. China*
† These authors contribute equally to this paper and should be considered as co-first author.

and so on. On the one hand, nanoparticles-based photosensitizers have been developed including liposomes,[7] polymersome,[8] MOF materials,[9] magnetic materials[10] and protein adducts.[11] However, these nanoencapsulation systems suffer from few limitations such as drug leakage, low drug loading efficiency, and overdosage of the inert matters. On the other hand, many photosensitizers have been chemically conjugated to functional molecules, such as lipid, fatty acid, or antibody, which could tune hydrophilicity/hydrophobicity or surface charges of photosensitizers. Especially, fatty acid, carbohydrate, protein and monoclonal antibodies have been conjugated to photosensitizers to improve photosensitizers targeting accumulations and distribution.[11–14] Different with chemical surfactants, microbial bio-surfactant may bring new possibilities for photosensitizer delivery. Microbial glycolipids such as rhamnolipids, cellobioselipids or sophorolipids have demonstrated outstanding biological application such as antifungal,[15] antibacterial,[16,17] anti-HIV,[18] and anticancer[19,20] properties. The synergistic effect of the sugar and lipid moieties could produce amphiphilic structure, which could contribute to their antibacterial effect through possible plasma membrane disruption mechanism, cell lysis and possible leakage.[21–23] Therefore, glycolipid conjugated to cationic photosensitizers would promote photosensitizers accumulation due to triple factors, such as high affinity to cell surface, hydrophobic association with lipids, and electrostatic attraction. Recently, Humblot *et al.*[24,25] have disclosed that the sophorose head group is able to damage both Gram+ and Gram−bacterial envelope, even though Gram−bacteria have an additional outer lipid membrane and lipopolysaccharide layer. Therefore, glycolipid conjugated photosensitizers could deliver photosensitizers into intracellular environment.

Herein, we propose a kind of photosensitizers modification protocol with sophorolipids, which could produce efficient accumulation and enhance anti-bacterial photodynamic therapy due to the affinity of sophorose to bacterial envelope. As illustrated in Fig. 1(A), photosensitizers toluidine blue has been conjugated to sophorolipid through classic EDC (1-(3-dimethylaminopropyl)-3-ethylcarbodiimide hydrochloride) activation method. The solution and photo-physical properties such as surface tension, micro-polarity, UV-vis absorption and fluorescence emission spectra have been recorded. The APDT efficiencies with free TB and SL-TB conjugates against *S. aureus* and *P. aeruginosa* have been demonstrated. Comparing with free TB, the accumulation and APDT targeting protein of SL-TB conjugates have been disclosed through fluorescence spectra/microscopy and protein electrophoresis.

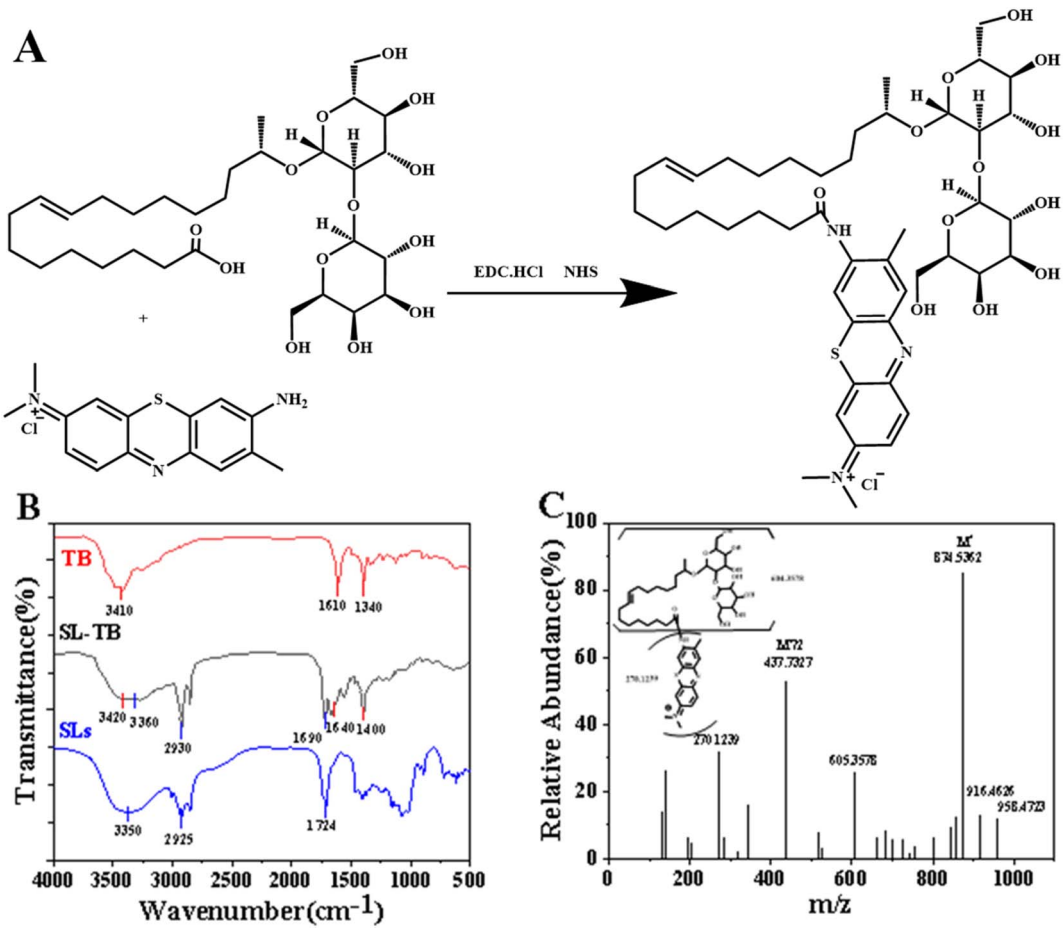

Fig. 1 Synthesis and structural characterization of sophorolipid-toluidine blue conjugates. (A) Synthesis diagram of sophorolipid-toluidine blue conjugates; (B) FT-IR spectra; (C) electrospray ionization high resolution mass spectra.

2. Experimental

2.1 Materials

Acidic sophorolipid (SLs) was prepared according to the methods reported by Song *et. al*.[26] Toluidine blue, 1-(3-dimethylaminopropyl)-3-ethylcarbodiimide hydrochloride (EDC-HCl), *N*-hydroxysulfosuccinimide (NHS), pyrene, 9,10-diphenylanthracene were purchased from Aladdin Regent Co., Ltd (Shanghai, China). Hydrochloric acid, methanol, chloroform, deuterated water, deuterated dimethyl sulfoxide, dimethyl sulfoxide were supplied by Sinopharm Chemical Reagent Co., Ltd. China. All other chemicals were supplied by Aladdin Regent Co., Ltd (Shanghai, China) and Macklin Inc. (Shanghai, China) unless otherwise mentioned and used as received without further purification. Ultrapure water (18.2 MΩ cm^{-1}) used in the experiments was prepared from a Millipore water purification system.

P. aeruginosa (CCTCC No.: M2017494 from Prof. Shuang Li, Nanjing Tech University) and *S. aureus* (CICC No.: 21600 from Dr Lixian Xu, the second affiliated hospital of Nanjing medical university) were selected as Gram− and Gram+ strains to demonstrate antibacterial photodynamic efficiencies, respectively.

2.2 Methods

2.2.1 Synthesis and characterization of sophorolipid-toluidine blue (SL-TB) conjugates. SL-TB conjugates were synthesized according to the classic EDC activation protocols. Firstly, equimolar EDC·HCl and *N*-hydroxy-succinimide (NHS) were added into sophorolipid solution (0.7 mmol in 100 mL H_2O) at room temperature. Then, the pH of transparent solution was adjusted to 5.0 using HCl and NaOH (1 mol L^{-1}), and the reactant solution was stirred to proceed carboxyl group activation at 0 °C for 30 min. Secondly, toluidine blue (0.5 g) was added slowly into the above solution and dissolved fully at 30 °C. Then the mixed solution was reacted at 30 °C for 24 h away from light. Finally, extracted by chloroform-methanol mixed solvent (10 : 1), the products SL-TB could be obtained through rotary evaporation and vacuum drying, and kept in a moisture-free desiccator before use. SL-TB conjugates were dissolved in DMSO-d6 and evaluated by ^1H nuclear magnetic resonance (NMR) analyses (Varian, Palo, Alto, USA, 400 MHz). FT-IR spectra (Brucker, Germany) were recorded from 400–4000 cm^{-1} with a resolution of 2 cm^{-1} at room temperature. Samples were mixed with KBr and tabletted before testing. Electrospray ionization high resolution mass spectra (ESI-HRMS) were obtained on Shimazu LCMS-IT-TOF system.

NMR (400 MHz) δ 9.31 (s), 7.63 (s), 7.44 (d, $J = 4.8$ Hz), 7.37 (s), 7.28 (s), 6.28 (d, $J = 31.7$ Hz), 5.46 (d, $J = 12.2$ Hz), 5.38 (d, $J = 15.9$ Hz), 5.30 (dd, $J = 16.6$, 9.6 Hz), 4.37 (s), 4.20 (d, $J = 1.4$ Hz), 4.05–3.91 (m), 3.77–3.44 (m), 3.31–2.98 (m), 2.85–2.70 (m), 2.25–2.21 (m), 2.11–1.95 (m), 1.52–1.17 (m), 0.84 (d, $J = 0.7$ Hz). ESI–HRMS [*m*/*z*]: 874.5362 (M^+), 437.7327(M^+/2).

2.2.2 Spectrometric methods. Due to the low solubility in water, SL-TB conjugates were dissolved in mixed solvent of DMSO and water (1 : 9, mass ratio). The electronic spectra of free and conjugated SL-TB solution (10 μmol L^{-1}) were recorded from 400–800 nm using UH3000 UV-Vis spectrophotometer (Hitachi, Japan), equipped with quartz cells. The fluorescence emission spectra of free and conjugated SL-TB solution (3 μmol L^{-1}) were recorded from 640 nm and 800 nm excited at 624 nm by spectrophotometer (F-7000, Hitachi).

2.2.3 Surface properties. The surface tension curves of sophorolipid and SL-TB conjugates were measured over the automatic tensionmeter (BZY-3B, Shanghai Hengping instruments Co.) at room temperature according to our previous reported method.[27] The thermodynamic parameters, including the minimum surface tension, critical micelle concentration (CMC), the minimal molecular cross-sectional area and the maximal surface excess concentration, were calculated according to the classic methods based on the surface tension curves.

The micropolarity in micelles has been disclosed by the fluorescence methods with pyrene as probes. Excited at 240 nm, the emission spectra from 350 nm to 420 nm were recorded, and the intensity at 373 nm and 384 nm were used to calculate I_1/I_3, which could be related to the micropolarity of conjugated photosensitizer assembly.

2.2.4 Light-triggered productivity of singlet oxygen species ($^1O_2$). Singlet oxygen productivity has been evaluated through 9,10-diphenylanthracene oxidation reaction. During experiments, 40 mL oxygen-saturated acetonitrile solution of 9,10-diphenylanthracene(100 μM) and photosensitizers (4 mM, equivalent to toluidine blue) was illuminated with a LED light source (660 nm, 30 mW cm^{-2}, Shenzhen Sanxin Optoelectronic Co., Ltd). The absorption spectra of 9,10-diphenylanthracene solution illustrated with different time were recorded by UH3000 UV-Vis spectrophotometer equipped with quartz cells. The intensity at 372 nm was used to calculate singlet oxygen production kinetics.

2.2.5 *In vitro* antibacterial photodynamic activity. The antibacterial photodynamic efficiency of free and conjugated SL-TB photosensitizers has been tested *in vitro* against Gram-positive *S. aureus* and Gram-negative *P. aeruginosa* bacteria as model strains according to our previous report.[28] The cell viability was determined by counting the CFU on the agar plate at the most appropriate dilution gradient. As a control, the bacterial suspensions were treated with soroholipid, SL-TB in dark and antibiotics cefixime (for *P. aeruginosa*) and vancomycin (for *S. aureus*). Three independent experiments were performed simultaneously and two replicates were plated for each condition.

2.2.6 *In vitro* cytotoxicity assay. CCK-8(Cell Counting Kit-8) was used to evaluate the cytotoxicity of SL-TB and TB to L929 mouse fibroblast cells(Yi Fei Xue Biotechnology, Nanjing, China). In brief, L929 cells(1×10^5 cells per mL) were inoculated onto 96-well plates and cultured in Dulbecco's Modified Eagle Medium(DMEM, less sugar). After 1 h, the sterilized photosensizers solutions (400 μM, equivalent TB) were added to 96-well plates containing cells, and then were exposed to 660 nm LED light at 30 mW cm^{-2} for 40 min. The mixture was incubated at 37 °C and 5% CO_2 for 24 h, 48 h, 72 h. After incubation, CCK-8 was added to each well and incubated for 1 h. The absorbance at 490 nm was measured by enzyme

labeling instrument and recorded as OD_{sample}. The absorbance of the blank group at 490 nm was recorded as $OD_{control}$ as a control. Three parallel samples were used in each experiment to ensure the validity of the results.

2.2.7 The cellular bioaccumulation of photosensitizers. The bioaccumulation of free TB and conjugated SL-TB into *P. aeruginosa* and *S. aureus* were measured according to our previous reports[29] with minor modification. Specifically, the bacteria suspension (CFU 10^{11} cells per mL) was firstly incubated with free or conjugated TB (400 mM) for 1 h at room temperature away from light. Then the bacterial cells were collected by centrifugation at 10 956 × *g* for 10 min. The obtained bacterial cells were washed triple with PBS, dispersed in PBS and subjected to record the fluorescence images by a fluorescence microscope (Ti2, Nikon) with excitation wavelengths of 633 nm. In order to quantify the photosensitizer on cell surfaces, the above washed bacterial cells were disrupted by ultrasonic cell grinder for 10 min, and the supernatant was collected by centrifugation at 10 956 × *g* for 10 min at 4 °C. The fluorescence spectra of the supernatant were recorded, and the accumulation of free or conjugated SL-TB was quantitatively calculated according to the standard curves.

2.2.8 Protein electrophoresis (SDS-PAGE). *P. aeruginosa* was selected to disclose the possible APDT mechanism with free and conjugated SL-TB. The equal volume of bacterial suspension (CFU 10^{11} cells per mL) and photosensitizer (400 mM) were mixed, incubated in dark for 30 minutes and then illustrated by 660 nm LED light for 40 min. The bacteria cells were collected through centrifugation and the fragmentation were performed through disruption by ultrasonic cell grinder. The fragmentation mixture was separated through centrifugation at 10 956 × *g* for 30 min. The intracellular protein (supernatant section) and membrane protein (precipitate section) analyses were performed by SDS-PAGE (EPS300, Tanon) with homemade SDS polyacrylamide gels (12%). Gel images were acquired using the GS-800 calibrated imaging densitometer (Bio-Rad). Apparent molecular weights and band intensities were recorded using the Quantity One v4.6.9 software (Bio-Rad). All samples were analyzed in triplicate.

3. Results and discussion

3.1 Synthesis and characterization of SL-TB conjugates

As shown in Fig. 1(A), SL-TB conjugates were synthesized by a facile one-pot EDC/NHS coupling reaction between amine group of toluidine blue and carboxyl group of sophorolipid. The chemical structure of SL-TB conjugates has been characterized by FT-IR, ESI-HRMS and ^{1}H NMR. As shown in Fig. 1(B), the absorption at 2930 cm^{-1} and 2853 cm^{-1} could be ascribed to the anti-systemic and systemic stretching vibration of C–H in C=C structure of unsaturated fatty acid. Comparing with free TB, the absorption at 1720 cm^{-1} could be ascribed to stretching vibration of C=O of amide bonds in SL-TB conjugates. In contrast, sophorolipid showed the absorption at 1724 cm^{-1}, which could be indexed to C=O bond of carbonyl group of the SL carboxylic acid. Meanwhile, the absorption at 1640 cm^{-1} and 1532 cm^{-1} demonstrated further the amide bond formation. In addition, the wide absorption between 3600 cm^{-1} and 3000 cm^{-1} could be indexed to the associated hydroxyl groups of sophorose in sophorolipid. Compared with TB, the wavenumbers of –C–N stretching vibration and bending vibration of –NH of SL-TB have increased, which may be attributed to the effect of the amide. From Fig. 2(A), ^{1}H NMR analysis confirmed the successful toluidine blue conjugation to sophorolipid due to the appearance of the broad peak at 9.2 ppm. The peak represents the hydrogen atom on the amide group of SL-TB. The signals of 0.8–2.0 ppm indicated the presence of alkane chain of sophorolipid. The peak at 3.0–4.3 ppm could be ascribed to –OH and –CH– on the sugar rings of sophorolipid. Meanwhile, the peak at 5.3 ppm belonged to hydrogen atoms of –CH=CH– and the peaks at 6.1–7.5 ppm were attributed to the hydrogen signals on the aromatic rings of toluidine blue. Fig. 1(C) was the high resolution mass spectrum of SL-TB, which showed that the 874.5362 signal represented the molecular weight of SL-TB positive ions. In addition, the 437.7327 fragment peak was attributed to half of the molecular weight of SL-TB positive ions. These results demonstrated the successful synthesis of sophorolipid-toluidine blue conjugates.

3.2 Interfacial and solution assembly

The surface tension curves of sophorolipid and SL-TB conjugates were measured and the results have been illustrated in Fig. 3(A). From Fig. 3(A), both sophorolipid and SL-TB conjugates showed the minimum surface tension is 40.1 mN m^{-1}. Moreover, comparing with free sophorolipid, conjugated sophorolipid-toluidine blue shows a more rapid decline rate, which indicated that sophorolipid-toluidine blue had higher surface activity. Calculated from the surface tension curves, the critical micelle concentration (CMC) of conjugated SL-TB as shown in Fig. 3(A) is 1.75×10^{-4} mol L^{-1}, which is significantly lower than that of sophorolipid, 2.99×10^{-4} mol L^{-1}.

According to the classic Gibbs adsorption isothermal equation,[30] the series of thermodynamic parameters such as the maximal surface excess concentration Γ_{max} and the minimal molecular cross-sectional area at the air–water interface (A_{min}) at the CMC have been calculated. Free sophorolipid gives A_{min} = 63.14 Å^2, and conjugated SL-TB gives the decreased A_{min} = 55.54 Å^2, suggesting that the molecular volume of SL-TB decreases due to phenothiazine structure packing of toluidine blue. The larger Γ_{max} value also affirm that more SL-TB molecules could accumulate more compactly on the air/water interface due to the higher packing density.

In order to disclose the various micelle micropolarity of free TB and conjugated SL-TB, the fluorescence spectra with pyrene as the probe have been recorded and shown in Fig. 3(B). Comparing with free TB in pure water, the conjugated SL-TB showed enhanced emission intensity. Moreover, I_1/I_3 value corresponding to free TB and conjugated SL-TB are 1.88 and 1.59, respectively. The lower I_1/I_3 value indicated that conjugated SL-TB could create more hydrophobic microenvironments for pyrene molecules, which demonstrated the amphiphilicity of conjugated SL-TB.

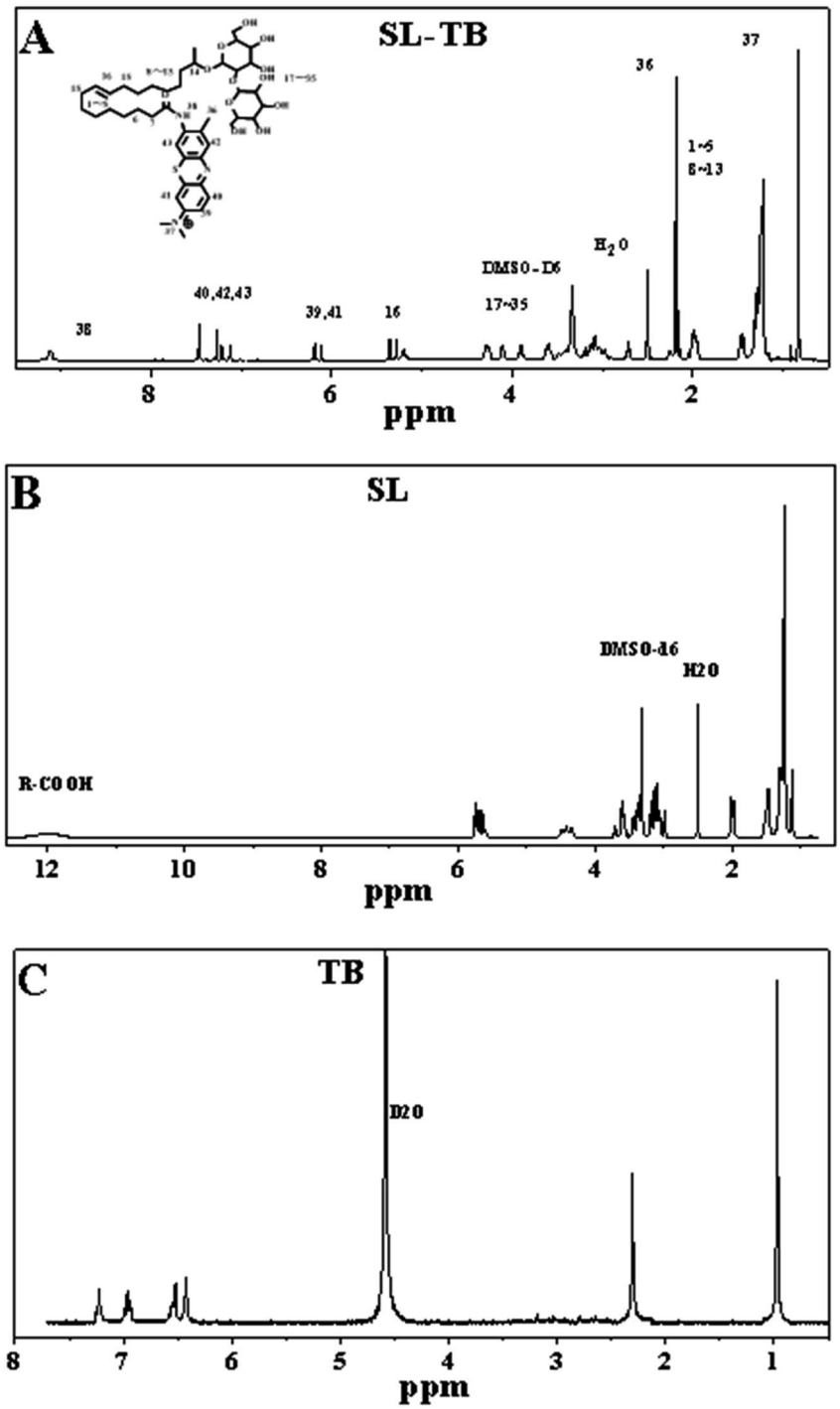

Fig. 2 ^{1}H NMR spectra of sophorolipid-toluidine blue conjugates (A), sophorolipid (B) and toluidine blue (C).

3.3 Photophysical properties of SL-TB conjugates

When TB was modified with sophorolipid, the lipophilicity would be improved and the solubility in water would decrease. Therefore, the photophysical properties of conjugated SL-TB in mixed solvent of DMSO/water were studied and the corresponding results have been shown in Fig. 4. From Fig. 4(A), the absorption intensity increased gradually with DMSO content increasing, which indicated that absorption of conjugated SL-TB in lower polar solvent had been enhanced. Meanwhile, the maximum absorption peak of SL-TB in DMSO/water (1 : 9) occurred at 645 nm, and the maximum absorption peak of SL-TB gradually blue-shifted to 640 nm with DMSO increasing. Meanwhile, as shown in Fig. 4(B), the fluorescence intensity of SL-TB conjugates also increased with the solvent polarity decrease, and the fluorescence intensity in the DMSO solvent was significantly stronger. Moreover, with DMSO increasing,

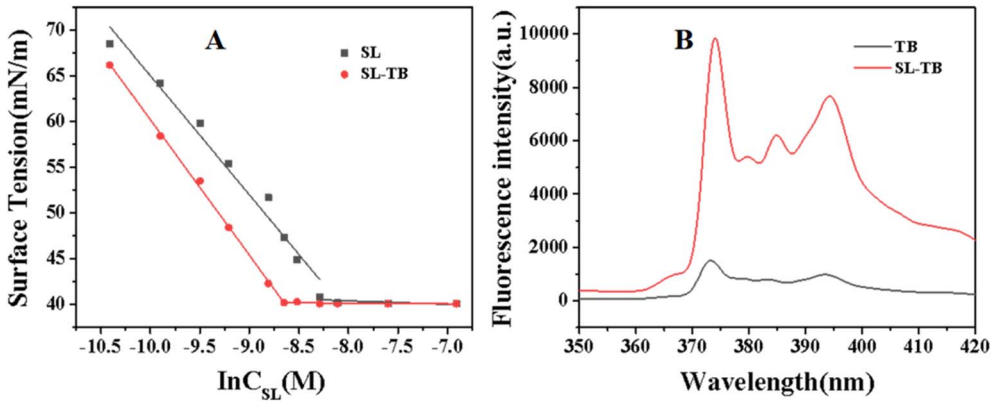

Fig. 3 The interfacial and solution assembly of sophorolipid-toluidine blue conjugates. (A) The surface tension curves of sophorolipid and sophorolipid-toluidine blue conjugates; (B) fluorescence spectra with pyrene as the fluorescent probe. Concentration: 3 μmol L^{-1}.

the maximum emission peaks of SL-TB solutions red-shifted from 653.8 nm to 657.2 nm. In addition, the absorption and the fluorescence intensity of TB showed a slight change with DMSO content increasing in Fig. 4(C) and (D). The maximum absorption peaks and the maximum emission peaks of TB showed the same trend as SL-TB, which could be attributed to the solvent effect.

Although the concentration of SL-TB in different solutions remained the same values, the fluorescence and absorption intensity increased with the increase of DMSO content, which may be attributed to the different aggregation states of molecules in different solvents. Amphiphilic SL-TB molecules could aggregate to form micelle in aqueous solution due to hydrophobic association. According to Rijcken's results,[31] the dye

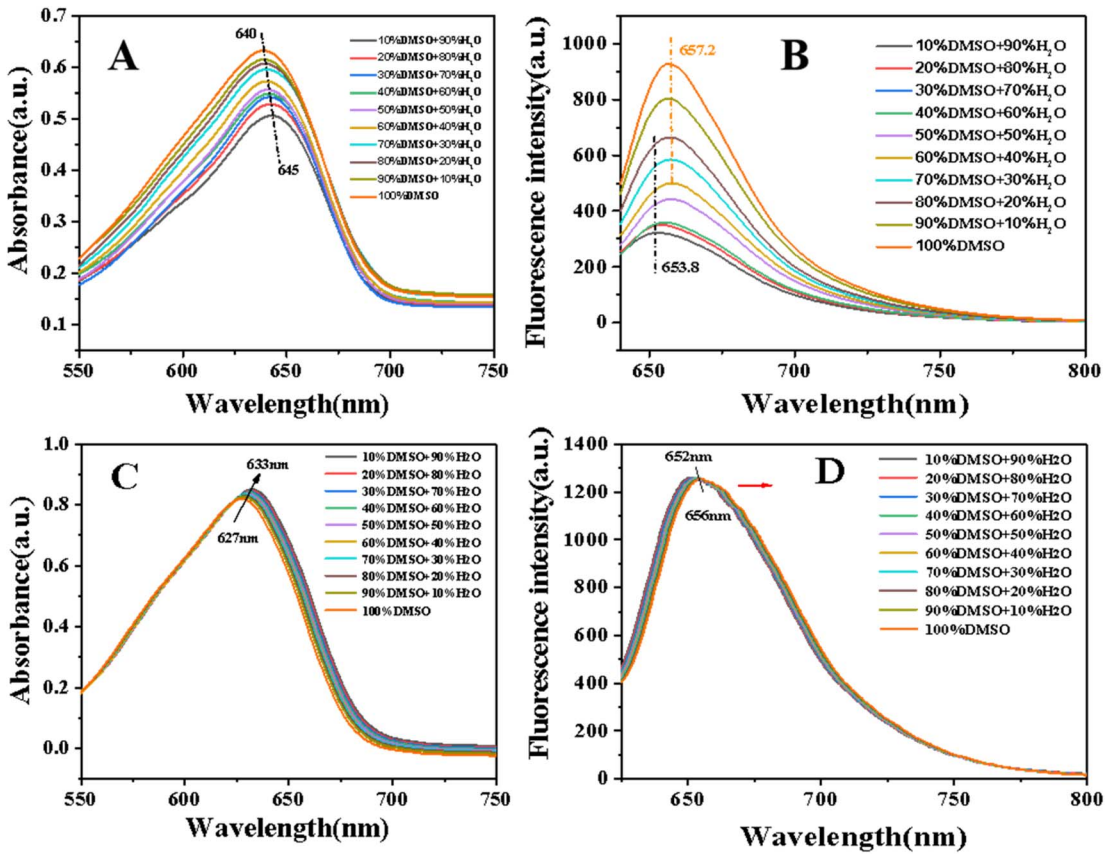

Fig. 4 The photophysical properties of free toluidine blue and sophorolipid-toluidine blue conjugates. (A) UV-vis absorption spectra of SL-TB in different solvents. Concentration: 10 μmol L^{-1}. (B) The fluorescence emission spectra of SL-TB in different solvents. Concentration: 3 μmol L^{-1}. (C) UV-vis absorption spectra of TB in different solvents. Concentration: 10 μmol L^{-1}. (D) The fluorescence emission spectra of TB in different solvents. Concentration: 3 μmol L^{-1}.

locating in the micelle interior microenvironment showed the decreased absorption. As we know, the fluorescence quench effect would appear when dye molecules aggregation increases.[32] Therefore, with DMSO content increasing, the SL-TB molecules aggregation in the solution gradually decreased, and the absorption and fluorescence intensity increased. Moreover, the absorption and emission maxima of TB and SL-TB showed the same shift tendency, which could be related merely to the variation of the refractive index of the mixed solvent medium.

3.4 Singlet oxygen production kinetics

9,10-Diphenylanthracene could be specifically oxidized by singlet oxygen $^1O_2$, and the absorption decay could be used to calculate singlet oxygen productivity kinetics. The absorbance of 9,10-diphenylanthracene at 372 nm was measured and the kinetics have been fitted and plotted in Fig. 5. From Fig. 5(A), with irradiation time increase, the absorbance at 372 nm decreased gradually for both free and conjugated TB. As shown in Fig. 5(B), the absorbance ln (A/A_0) at 372 nm of 9,10-diphenylanthracene was plotted as the function of irradiation time, and the singlet oxygen kinetics constant could be obtained from the slope of the fitted pseudo-first-order plots. According to the fitted results, the rate constant k of singlet oxygen productivity provided by free TB is -0.25 min^{-1}, and the rate constants k of conjugated SL-TB was -0.29 min^{-1}. These results indicated that conjugated SL-TB showed the increased singlet oxygen productivity comparing with free TB. According to the photodynamic mechanism,[33] the photosensitizers under irradiation could be excited from singlet ground state to its singlet excited state. From the excited state, a fraction of the excited state could be transformed *via* intersystem crossing(ISC) to the long-life triplet excited state, which could generate reactive oxygen species(ROS), either producing free radicals or radical ions through electron transfer (type I mechanism), or forming singlet oxygen through energy-transfer to molecular oxygen (type II mechanism). Therefore, the increased singlet oxygen productivity in present research could be induced by increased excitation quantum yield of conjugated SL-TB, as disclosed by the increased fluorescent intensity in DMSO-water mixed solvents shown in Fig. 4. The conjugation of sophorolipid could improve the lipophilicity of photosensitizers, and increase the fluorescence emission capability and singlet oxygen productivity.

3.5 *In vitro* antibacterial photodynamic efficiency and biocompatibility

The anti-bacterial photodynamic efficiency of SL-TB conjugates on *P. aeruginosa* and *S. aureus* were evaluated using a classic colony counting method. Fig. 6(A) and (B) shows digital images of *P. aeruginosa* and *S. aureus* culture plates after various treatments, respectively. As shown in the histogram in Fig. 6(C), sophorolipid showed moderate antibacterial capability, and several literature have reported that sophorolipids had a bactericidal effect towards Gram-positive and Gram-negative strains.[34–36] According to Marchant's results,[36] the antimicrobial mechanism of sophorolipids is closer to that of antibiotic drugs, which was considered to be cell wall/membrane lysis. Recently, Bhattacharyya *et. al.*[37] reported that sophorolipid induced ROS generation in *C. albicans* leading to mitochondrial dysfunction and ER stress followed by the release of Ca^{2+} ions (from the ER lumen) that entered mitochondria and further magnified ROS generation leading to cell death. Humblot *et. al.* reported that sophorose head group of sophorolipid was able to damage both Gram+ and Gram−bacterial envelopes, even though Gram−bacteria has an additional outer lipid membrane and lipopolysaccharide layer.[24,25] Comparing with sophorolipid, SL-TB conjugates in dark showed the weaker antibacterial efficiency, which indicated that the free carboxyl group of sophorolipid was also very important for antibacterial process. When treated with free toluidine blue and light, the antibacterial efficiencies defined as CFU reduction in $\log_{10}$ unit were 4.5 and 7.9 for *P. aeruginosa* and *S. aureus*, respectively, much higher than antibiotics groups in Fig. 6(C). Interestingly, conjugated SL-TB showed the improved antibacterial efficiencies, $\log_{10}$ unit 6.3 and 9.7 for *P. aeruginosa* and *S. aureus,* respectively. In view of lower singlet oxygen quantum yield of SL-TB conjugates than

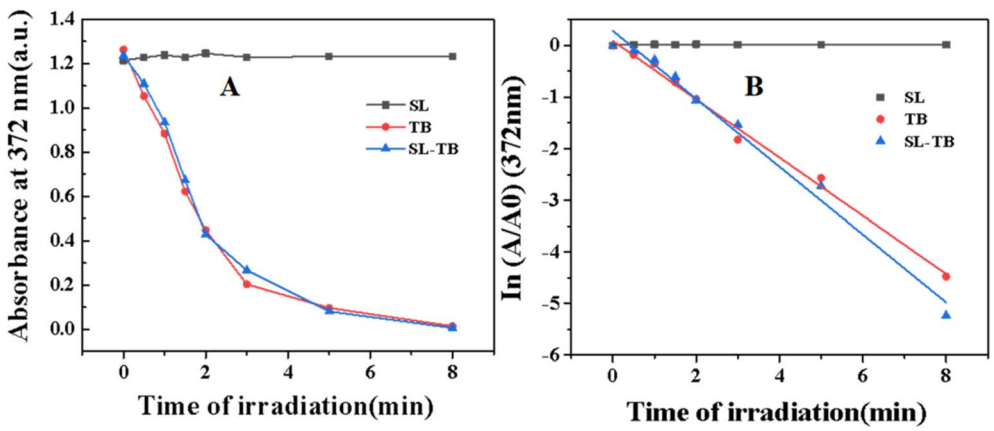

Fig. 5 Singlet oxygen productivity kinetics of free TB and conjugated SL-TB detected by 9,10-diphenylanthracene oxidation. (A) The absorbance decay at 372 nm with different irradiation time; (B) singlet oxygen productivity fitted with a pseudo-first order kinetics.

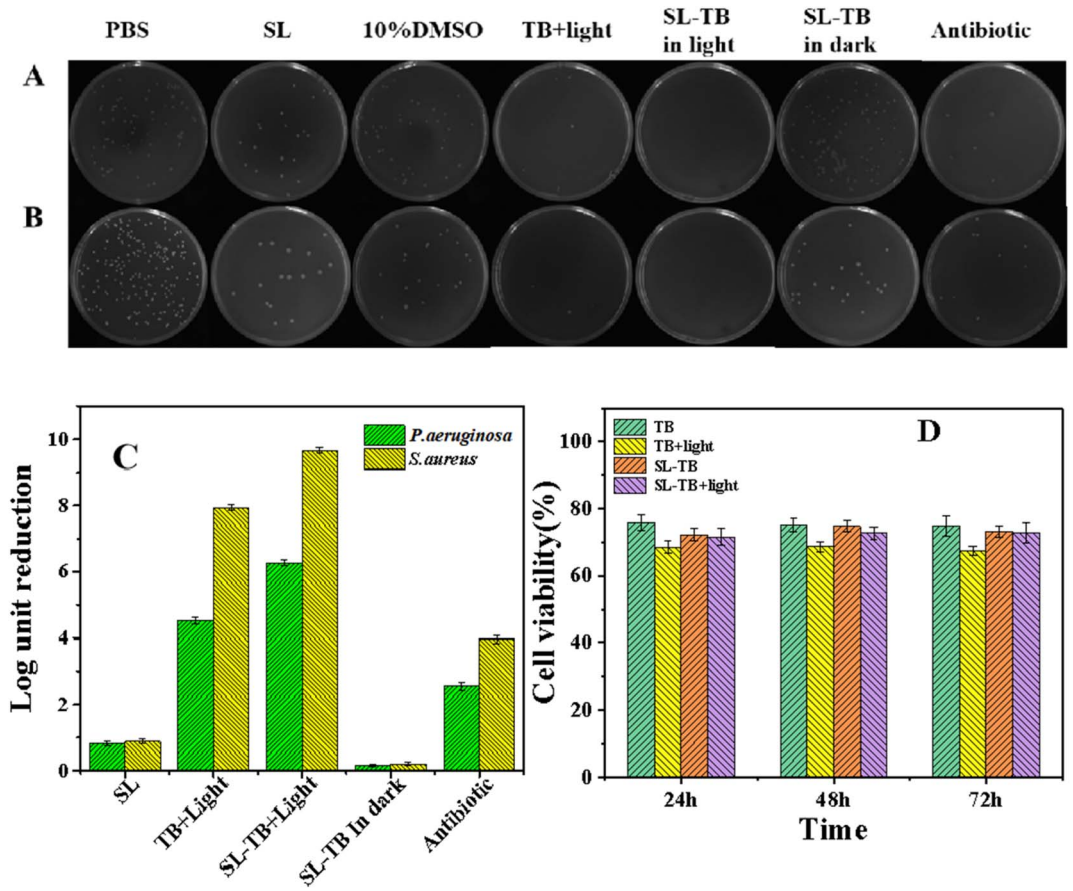

Fig. 6 *In vitro* APDT activity and biocompatibility patterns. Photographs of plate samples of Gram-negative *P. aeruginosa* (A) and Gram-positive *S. aureus* (B) treated with APDT. For APDT, bacteria were incubated with SL-TB or free TB (400 μM, equivalent TB) and exposed to 660 nm LED light at 30 mW cm^{-2} for 20 min. Antibiotics vancomycin and cefixime (100 mg L^{-1}) were used for *S. aureus* and *P. aeruginosa*, respectively, as control. (C) APDT activity was quantitated by counting colony forming units per milliliter (CFU mL^{-1}) and reduction in the log unit compared to the sophorolipid group and antibiotics group. (D) Viability of L929 mouse fibroblast cells cultured with different photosensiziters for various time. Fibroblast cells were incubated with SL-TB or free TB (400 μM, equivalent TB) and exposed to 660 nm LED light at 30 mW cm^{-2} for 40 min.

free TB as shown in Fig. 5, the enhanced antibacterial activity could be ascribed to the increase of photosensitizer bioaccumulation. These results demonstrated that SL-TB conjugates could be accumulated more on bacterial cells, and produce higher antibacterial activities through photodynamic mechanism.

In order to demonstrate the biocompatibility patterns of free TB and conjugated photosensitizers SL-TB on healthy human cells, the influence of the photodynamic treatment on L929 mouse fibroblast cells viability has been demonstrated as shown in Fig. 6(D). With the same photosensitizers concentration to APDT experiments, the survival rates were over 75% when the cells were cultured with free TB without light, and the photodynamic treatment of free TB has decreased the cell viability to 68%. In comparison, the survival rates remained over 70% whether or not SL-TB is exposed to light, which demonstrated that conjugated SL-TB has lowered cytotoxicity comparing with free TB. Thus, these results suggest that conjugated photosensizizers SL-TB has acceptable *in vitro* biocompatibility and would find promising biomedical applications.

3.6 Photosensitizers accumulation over bacterial cells

To assess whether the enhanced cell viability reduction by SL-TB was related to photosensitizer accumulation mediated by sophorolipid, *S. aureus* and *P. aeruginosa* were cultured with free TB and conjugated SL-TB and the fluorescence images of stained bacterial cells were recorded and shown in Fig. 7(A) and (B). Since cationic toluidine blue could be accumulated on cells of *S. aureus* and *P. aeruginosa* through electrostatic attraction, the fluorescence emission of toluidine blue can be taken as the indicator of photosensitizers accumulation. The stronger and more red areas in Fig. 7(A) and (B) showed that SL-TB conjugates could be accumulated with higher concentration over *S. aureus* and *P. aeruginosa* than free toluidine blue. In order to compare quantitatively the accumulation of different photosensitizers on cells, we characterized them by fluorescence quantitative method, and the results are summarized in the histogram shown in Fig. 7(C). From Fig. 7(C), the accumulations of free toluidine blue on *P. aeruginosa* and *S. aureus* were 462 and 827 nmol/10^{11} cells, respectively. In comparison, those of conjugated SL-TB on *P. aeruginosa* and *S. aureus* were increased

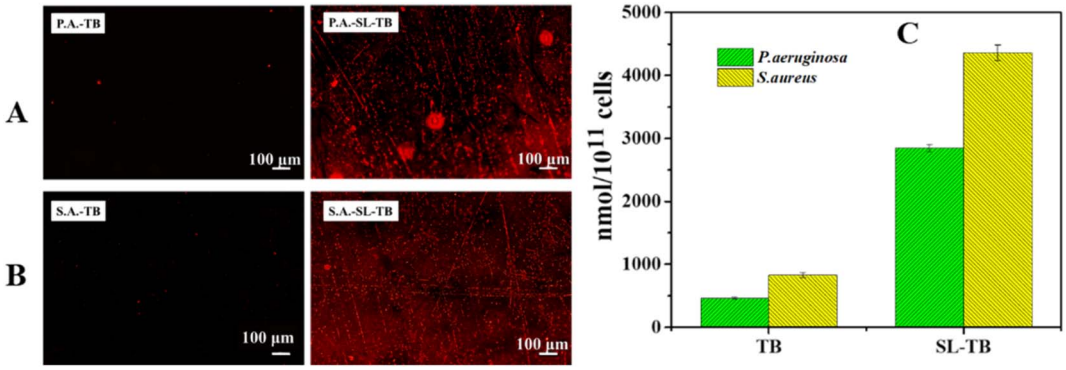

Fig. 7 The cellular accumulations of free TB and conjugated SL-TB by *S. aureus* and *P. aeruginosa*. (A) Fluorescence microscope photographs of *P. aeruginosa* incubated with free TB or conjugated SL-TB. (B) Fluorescence microscope photographs of *S. aureus* incubated with free TB or conjugated SL-TB. (C) The quantitative determination of free TB and conjugated SL-TB accumulations over *S. aureus* and *P. aeruginosa* quantified by fluorescence spectra methods.

obviously, that is 2850 and 4360 nmol/10^{11} cells, which demonstrated that conjugated SL-TB photosensitizers could be accumulated more efficiently due to triple factors, such as sophorose affinity to cell membrane, hydrophobic association with plasma membrane and electrostatic attraction. According to Borsanyiova's report,[38] sophorolipid could soften *P. aeruginosa* membrane and improve the membrane permeation, which could be in favor of photosensitizers transmembrane delivery. Besides, alkyl chain of sophorolipid could interact with lipids of plasma membrane, which would improve the binding of photosensitizers with bacterial cells.

3.7 SDS-PAGE

To demonstrate the different APDT targeting objects in bacterial cells by free TB and conjugated SL-TB photosensitizers, the integrity of *P. aeruginosa* membrane and intracellular proteins was examined using SDS-PAGE technique as shown in Fig. 8. From membrane protein results in Fig. 8(A), conjugated SL-TB showed the similar protein chains to blank control, which indicated that conjugated SL-TB had little influence on membrane proteins. In comparison, free TB give lighter protein chains at 60, 97 and 116 kDa than those of blank control, indicating that free TB have damaged these protein through photodynamic process. Due to the cationic nature, free TB could accumulate to biological objects with negative charges through electrostatic attraction, produce singlet oxygen under light irradiation to damage transmembrane protein and lipid, and induce bacterial death. The intracellular proteins integrity treated with free TB and conjugated SL-TB gives the contrary results as shown in Fig. 8(B). Comparing with blank control, the intracellular proteins extracted from *P. aeruginosa* treated with free TB under light irradiation showed the similar protein

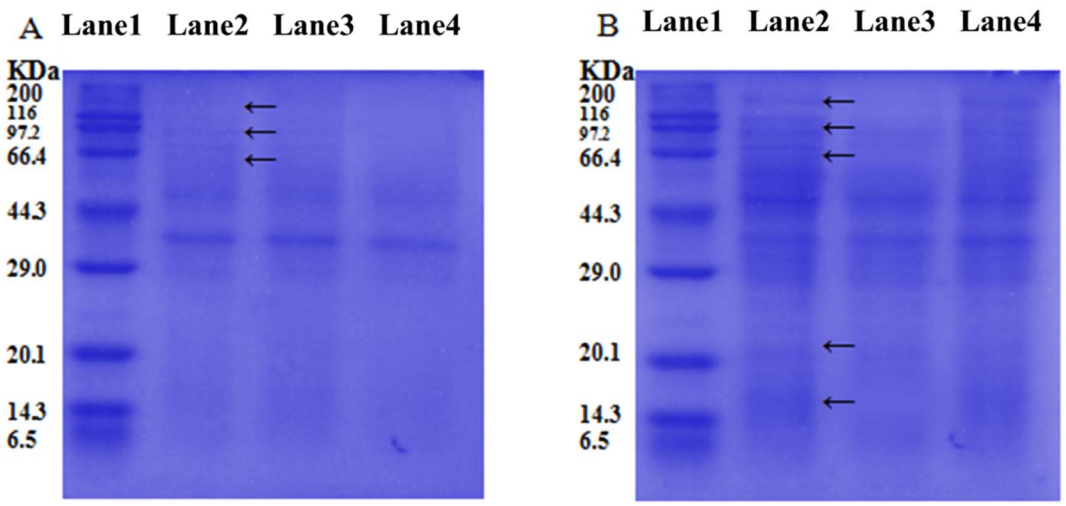

Fig. 8 SDS-PAGE of *P. aeruginosa* proteins after photodynamic treatment. (A) The protein fractions profiles of precipitate (membrane protein); (B) the protein fractions profiles of supernatant (intracellular protein). Cells were incubated with 400 μM of photosensitizer for 30 min in dark and irradiated with LED light (30 mW cm^{-2}) for 40 min. M: molecular weight marker. Black arrows indicate representative protein bands with different intensity after treatment. Lanes: (1) protein standard markers; (2) blank control; (3) treatment with conjugated SL-TB; (4) treatment with free toluidine blue.

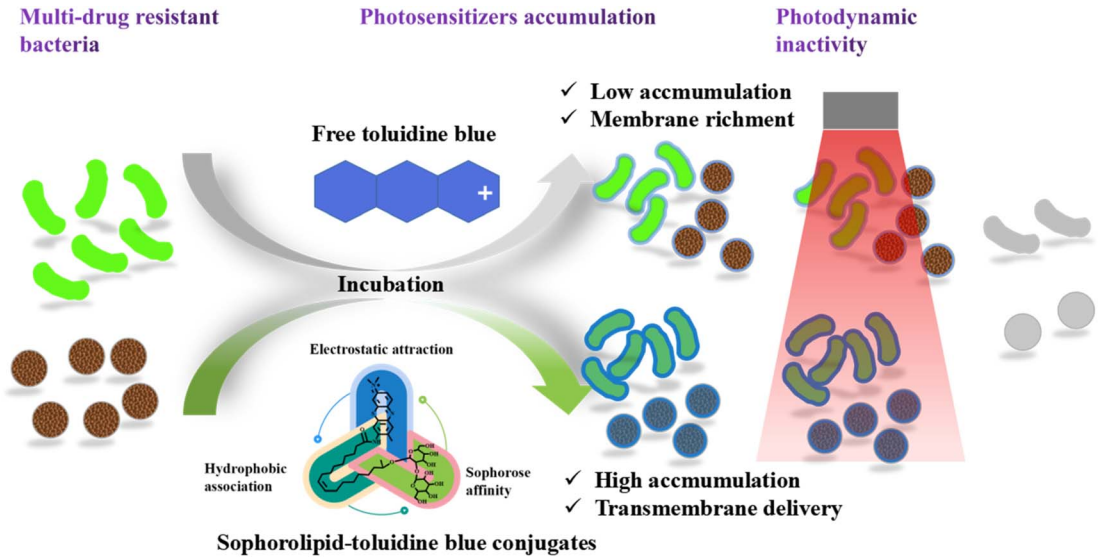

Fig. 9 A diagram of enhanced anti-bacterial photodynamic therapy induced by conjugated sophorolipid-toluidine blue.

profiles, which indicated that water soluble TB couldn't be accumulated into intracellular environment due to high diffusion resistance of plasma membrane. In comparison, almost all protein chains larger than 66 kDa have disappeared when *P. aeruginosa* treated with conjugated SL-TB under light irradiation, which indicated that a large amount of intracellular proteins have been degraded due to singlet oxygen oxidation from photodynamic process. These results demonstrated that conjugated SL-TB photosensitizers could transcellular accumulate in intracellular environment due to the transcellular advantages of microbial surfactants sophorolipid.

The clinical application of photodynamic therapy is always restricted by the low accumulation and poor targeting of photosensitizers, which could be solved through chemical modification of photosensitizers through conjugated with functional molecules, such as monoclonal antibody.[14] Generally, the antibacterial properties of glycolipid could be attributed to their permeabilization effect that destroys the integrity of the plasma membrane,[39] which could make bacteria more susceptible to antimicrobial agents. In view of the high affinity to bacterial cells,[40] sophorolipid was selected to conjugate to toluidine blue, and the possible APDT mechanism of SL-TB conjugates has been illustrated in Fig. 9. Toluidine blue is a kind of cationic photosensitizer, which could be accumulated over negative-charged bacterial cell surface through electrostatic interaction. However, these photosensitizers molecules could not diffuse across the lipid bilayer structure of cell membrane, and can only aggregate on the extracellular surface, which have been confirmed by the SDS-PAGE results of membrane proteins in Fig. 8. In contrast, SL-TB conjugates could be accumulated with higher concentration due to the triple factors, such as the high affinity of sophorose headgroup to cell membrane, hydrophobic association with plasma memtrane and electrostatic attraction. Moreover, the higher accumulation of SL-TB conjugates has been demonstrated by the fluorescence images and quantitative results in Fig. 7. Besides, SL-TB has produced enhanced APDT efficiency through targeting different objects with free toluidine blue. According to Otzen's reports,[41] the sophorose structure of sophorolipid can enter cells through disturbing cell membrane and increase the permeability. The SDS-PAGE results in Fig. 8 also demonstrated that SL-TB conjugates could destroy intracellular biological macromolecules, such as proteins, indicating that SL-TB has been transmembrane delivery due to sophorolipid carrying effect. Based on higher accumulation and intracellular delivery, conjugated SL-TB could produced enhanced antibacterial photodynamic therapy efficiency.

4. Conclusion

Anti-bacterial photodynamic efficiency is dependent on photosensitizers accumulation on targeting bacterial cells. In view of high affinity of sophorolipid to bacterial membrane and amphiphilic characteristics, sorphorolipid has been used to conjugate to hydrophilic toluidine blue, and to improve photosensitizers accumulation onto bacterial cells. Comparing with free TB, conjugated SL-TB could accumulate 6.2-fold and 5.3-fold on *P. aeruginosa* and *S. aureus*, respectively, comparing with free TB. Successively, conjugated SL-TB could reduce the CFU 6.3 $\log_{10}$ and 9.7 $\log_{10}$ for *P. aeruginosa* and *S. aureus*, respectively, higher than free TB of CFU 4.5 $\log_{10}$ and 7.9 $\log_{10}$. The present research would provide valuable information for developing more efficient photodrugs for photodynamic therapy and transcellular drug delivery formulation.

Author contribution

Xiaoxiao Gu: data curation, methodology, investigation. Lixian Xu: clinical research idea and data curation, writing – review & editing. Haoyang Yuan: conceptualization, methodology, review. Cailing Li: methodology, investigation. Juan Zhao: methodology, investigation. Shuang Li: microbacterial data

curation, funding acquisition. Dinghua Yu: supervision, data curation, project administration.

Conflicts of interest

The authors declare that they have no known competing financial interests or personal relationships that could have appeared to influence the work reported in this paper.

Acknowledgements

This work was supported by the National Key Research and Development Plan (No. 2021YFC2103800), the National Natural Science Foundation of China (No. 21576133), the Six Talent Peaks Project in Jiangsu Province (No. 2018-GDZB-196), and the Jiangsu Synergetic Innovation Center for Advanced Bio-Manufacture.

References

1 Q. Gao, L. Bao, H. Mao, L. Wang, K. Xu, M. Yang, Y. Li, L. Zhu, N. Wang, Z. Lv, H. Gao, X. Ge, B. Kan, Y. Hu, J. Liu, F. Cai, D. Jiang, Y. Yin, C. Qin, J. Li, X. Gong, X. Lou, W. Shi, D. Wu, H. Zhang, L. Zhu, W. Deng, Y. Li, J. Lu, C. Li, X. Wang, W. Yin, Y. Zhang and C. Qin, *Science*, 2020, **369**, 77–81.

2 S. Xu and Y. Li, *Lancet*, 2020, **395**, 1321–1322.

3 L. S. J. Roope, R. D. Smith, K. B. Pouwels, J. Buchanan, L. Abel, P. Eibich, C. C. Butler, P. S. Tan, A. S. Walker, J. V. Robotham and S. Wordsworth, *Science*, 2019, **364**, eaau4679.

4 Y. Zhu, M. Jović, A. Lesch, L. Tissières Lovey, M. Prudent, H. Pick and H. H. Girault, *Angew. Chem., Int. Ed. Engl.*, 2018, **57**, 14942–14946.

5 C. Årdal, M. Balasegaram, R. Laxminarayan, D. McAdams, K. Outterson, J. H. Rex and N. Sumpradit, *Nat. Rev. Microbiol.*, 2020, **18**, 267–274.

6 Y. Huang, W. Chen, J. Chung, J. Yin and J. Yoon, *Chem. Soc. Rev.*, 2021, **50**, 7725–7744.

7 G. Boccalini, L. Conti, C. Montis, D. Bani, A. Bencini, D. Berti, C. Giorgi, A. Mengoni and B. Valtancoli, *J. Mater. Chem. B*, 2017, **5**, 2788–2797.

8 C. Piccirillo, S. Perni, J. Gil-Thomas, P. Prokopovich, M. Wilson, J. Pratten and I. P. Parkin, *J. Mater. Chem.*, 2009, **19**, 6167–6171.

9 D. B. Tada, L. L. Vono, E. L. Duarte, R. Itri, P. K. Kiyohara, M. S. Baptista and L. M. Rossi, *Langmuir*, 2007, **23**, 8194–8199.

10 A. J. T. Naik, S. Ismail, C. Kay, M. Wilson and I. P. Parkin, *Mater. Chem. Phys.*, 2011, **129**, 446–450.

11 P. M. Pereira, J. J. Carvalho, S. Silva, J. A. Cavaleiro, R. J. Schneider, R. Fernandes and J. P. Tomé, *Org. Biomol. Chem.*, 2014, **12**, 1804–1811.

12 N. Malatesti, I. Munitic and I. Jurak, *Biophys. Rev.*, 2017, **9**, 149–168.

13 K. Smith, N. Malatesti, N. Cauchon, D. Hunting, R. Lecomte, J. E. van Lier, J. Greenman and R. W. Boyle, *Immunology*, 2011, **132**, 256–265.

14 J. Sandland and R. W. Boyle, *Bioconjugate Chem.*, 2019, **30**, 975–993.

15 S. Sen, S. N. Borah, A. Bora and S. Deka, *Microb. Cell Fact.*, 2017, **16**, 95.

16 S. Vasudevan and A. A. Prabhune, *R. Soc. Open Sci.*, 2018, **5**, 170865.

17 E. I. P. Delbeke, B. I. Roman, G. B. Marin, K. M. Van Geem and C. V. Stevens, *Green Chem.*, 2015, **17**, 3373–3377.

18 V. Shah, G. F. Doncel, T. Seyoum, K. M. Eaton, I. Zalenskaya, R. Hagver, A. Azim and R. Gross, *Antimicrob. Agents Chemother.*, 2005, **49**, 4093–4100.

19 L. Rodrigues, I. M. Banat, J. Teixeira and R. Oliveira, *J. Antimicrob. Chemother.*, 2006, **57**, 609–618.

20 S. Kithur Mohamed, M. Asif, M. V. Nazari, H. M. Baharetha, S. Mahmood, A. R. M. Yatim, A. S. Abdul Majid and A. M. S. Abdul Majid, *Indian J. Pharmacol.*, 2019, **51**, 45–54.

21 M. Sánchez, F. J. Aranda, J. A. Teruel, M. J. Espuny, A. Marqués, A. Manresa and A. Ortiz, *J. Colloid Interface Sci.*, 2010, **341**, 240–247.

22 V. Rondelli, L. Mollica, A. Koutsioubas, N. Nasir, M. Trapp, E. Deboever, P. Brocca and M. Deleu, *J. Colloid Interface Sci.*, 2022, **616**, 739–748.

23 J. Ortiz, A. Oliva, J. A. Teruel, F. J. Aranda and A. Ortiz, *J. Colloid Interface Sci.*, 2021, **597**, 160–170.

24 C. Valotteau, I. M. Banat, C. A. Mitchell, H. Lydon, R. Marchant, F. Babonneau, C. M. Pradier, N. Baccile and V. Humblot, *Colloids Surf., B*, 2017, **157**, 325–334.

25 C. Valotteau, C. Calers, S. Casale, J. Berton, C. V. Stevens, F. Babonneau, C. M. Pradier, V. Humblot and N. Baccile, *ACS Appl. Mater. Interfaces*, 2015, **7**, 18086–18095.

26 X. Ma, H. Li and X. Song, *J. Colloid Interface Sci.*, 2012, **376**, 165–172.

27 F. Hu, Y. Liu, J. Lin, W. Wang, D. Yu and S. Li, *Colloids Surf., B*, 2021, **200**, 111602.

28 J. Zhao, L. Xu, H. Zhang, Y. Zhuo, Y. Weng, S. Li and D. Yu, *Colloids Surf., B*, 2021, **207**, 111974.

29 H. Zhang, L. Xu, X. Gu, D. Yu and S. Li, *RSC Adv.*, 2023, **13**, 239–250.

30 L. Martinez-Balbuena, A. Arteaga-Jimenez, E. Hernandez-Zapata and C. Marquez-Beltran, *Adv. Colloid Interface Sci.*, 2017, **247**, 178–184.

31 C. J. Rijcken, J. W. Hofman, F. van Zeeland, W. E. Hennink and C. F. van Nostrum, *J. Controlled Release*, 2007, **124**, 144–153.

32 W. Li, J. Wang, Y. Xie, M. Tebyetekerwa, Z. Qiu, J. Tang, S. Yang, M. Zhu and Z. Xu, *Prog. Org. Coat.*, 2018, **120**, 1–9.

33 Q. Jia, Q. Song, P. Li and W. Huang, *Adv. Healthcare Mater.*, 2019, **8**, e1900608.

34 M. A. Díaz De Rienzo, P. Stevenson, R. Marchant and I. M. Banat, *FEMS Microbiol. Lett.*, 2016, **363**, fnv224.

35 V. A. I. Silveira, C. A. U. Q. Freitas and M. A. P. C. Celligoi, *J. Appl. Biol. Biotechnol.*, 2018, **6**(06), 87–90.

36 I. M. Banat, A. Franzetti, I. Gandolfi, G. Bestetti, M. G. Martinotti, L. Fracchia, T. J. Smyth and R. Marchant, *Appl. Microbiol. Biotechnol.*, 2010, **87**, 427–444.
37 F. Haque, N. K. Verma, M. Alfatah, S. Bijlani and M. S. Bhattacharyya, *RSC Adv.*, 2019, **9**, 41639–41648.
38 M. Borsanyiova, A. Patil, R. Mukherji, A. Prabhune and S. Bopegamage, *Folia Microbiol.*, 2016, **61**, 85–89.
39 A. Ramos da Silva, M. Manresa, A. Pinazo, M. T. García and L. Pérez, *Colloids Surf., B*, 2019, **181**, 234–243.
40 P. R. Franco Marcelino, J. Ortiz, S. S. da Silva and A. Ortiz, *Colloids Surf., B*, 2021, **207**, 112029.
41 D. E. Otzen, *Biochim. Biophys. Acta, Biomembr.*, 2017, **1859**, 639–649.